Volume 1 | Number 1 | Jan 2013 | Pages 1–100

PCCP

Physical Chemistry Chemical Physics
www.rsc.org/pccp

ROYAL SOCIETY OF CHEMISTRY

ROYAL SOCIETY OF CHEMISTRY

www.rsc.org/pccp

Origins of Tunable Photoluminescence from Graphene Quantum Dots Synthesized by Pulsed Laser Ablation

S. R. M. Santiago[1], T. N. Lin[1], C. T. Yuan[1], J. L. Shen[1]*, H. Y Huang[2] and C. A. J. Lin[2]

[1]Department of Physics and Center for Nanotechnology, Chung Yuan Christian University, Chung-Li 32023, Taiwan

[2]Department of Biomedical Engineering, Chung Yuan Christian University, Chung-Li 32023, Taiwan

One-step synthesis of graphene quantum dots (GQDs) has been implemented using pulsed laser ablation (PLA) with carboxyl-functionalized multiwalled carbon nanotubes (MWCNTs). The synthesized GQDs with an average size smaller than 3 nm were obtained by fragmentation of MWCNTs via oxidative cutting. The GQDs can generate tunable photoluminescence (PL) ranging from green to blue by controlling the PLA time. The PL spectrum (decay time) of the green GQDs remains unchanged under different excitation energies (emission energies), while that of the blue GQDs correlates with the excitation energy (emission energy). On the basis of the pH and temperature dependence of PL, we suggest that the localized intrinsic states associated with the sp^2 nanodomains and delocalized extrinsic states embedded on the GQD surface are responsible for blue and green emission in GQDs, respectively.

*Correspondence to: jlshen@ cycu.edu.tw

1. INTRODUCTION

Graphene is a two-dimensional material which consists of sp^2-bonded carbon atoms arranged in a hexagonal lattice. Graphene has attracted vast attention in science and technology in recent years due to its exceptional optical, electronic, thermal, magnetic and mechanical properties.[1-7] Owing to the lack of a bandgap, graphene has limitation on the

electronic and optoelectronic applications. The energy bandgap of graphene, however, can be generated by engineering of its shape, size and surface structure, resulting to graphene quantum dots (GQDs) or graphene nanoribbons (GNRs).[7-13] GQDs are graphene with nanoscale lateral dimensions with high surface to volume ratio.[14-17] GQDs possess characteristics such as low toxicity, robust chemical inertness, stable photoluminescence (PL), resistant to photo-bleaching, good surface grafting, and excellent solubility.[18-22] Owing to these characteristics, GQDs can be utilized for application in the fields of photovoltaics, photocatalysis, biomedical imaging, biological sensing, and drug delivery.[23-27] In general, two approaches have been used for synthesis of GQDs. One approach is the bottom-up method, wherein, carbonization or self-assembly of organic materials is implemented.[14,28] Another approach is top-down method, which is carried out through cutting, exfoliating, unzipping of carbon-based raw materials into the nanoscaled size of GQDs.[10,17-18,28] One of the top-down approaches called pulsed laser ablation (PLA) has gained great attention for the synthesis of GQDs. The PLA method uses a pulsed laser to irradiate the carbon based raw material that is deposited in water or in organic solvent, producing disintegrated particles with modified surfaces.[29-30] The PLA method is advantageous for one step, lesser synthesis time, good reproducibility, and minimal experimental set-up.[28-31]

Applications of GQDs are sometimes hindered by the limited PL wavelength from GQDs. It is therefore desirable to prepare GQDs with tunable PL. On the basis of the density-functional theory, the energy bandgap in functionalized GQDs can be varied by varying it size, edge, shape, defects, and functional groups.[7] Recently, the GQDs with variable emission wavelength have been implemented by using a diverse of coals having the graphene domains in different size and by controlling the cross-flow ultrafiltration through the membrane pore size and the reaction temperature of the oxidation process.[25,32] Although synthesis of GQDs with tunable PL can be implemented, the luminescence mechanism of GQDs is not conclusive. For example, the blue PL in GQDs has been associated with carbene-like triplet states, intrinsic free zigzag sites with carbon crystalline structures, or band-to-band π^*-π

transitions.[3,18] Also, the origin of the green PL in GQDs has been attributed to extrinsic defect states or the electronic transition from lowest unoccupied molecular orbits (LUMOs) to highest occupied molecular orbits (HOMOs).[5,18] Understanding the PL mechanism of GQDs with different wavelengths is expected to be essential for their possible applications in biomedicine, photocatalysis, and optical devices. In this study, we proposed a method of synthesizing GQDs from carboxyl-functionalized multiwalled carbon nanotubes (MWCNTs) via PLA. The wavelength of the PL of the synthesized GQDs can be easily tuned from green to blue by controlling the laser irradiation time in PLA. The structural, optical, and chemical properties of the synthesized GQDs were investigated by the transmission electron microscopy (TEM), PL, time-resolved PL, Ultraviolet-visible (UV-Vis) absorption, and X-ray photoelectron spectroscopy (XPS). A mechanism responsible for the blue and green PL of GQDs is proposed.

2.   EXPERIMENTAL SECTION

The precursor carboxyl-functional MWCNTs were prepared using noncovalent oxidative treatment.[33] A 0.0015 g of carboxyl-functional MWCNTs was dissolved in 1 ml of the deionized water in a quartz bottle and was thoroughly mixed using a vortex shaker with an angular velocity of 6000 rpm. Subsequently, MWCNTs-water solution was irradiated using an optical parametric oscillator (OPO) laser with an excitation wavelength of 415 nm, a frequency of 10 Hz, and energy of ~48 mJ. Concurrent with PLA, continuous mixing of the solution was carried out by a rotator with an angular velocity of 80 rpm. Various GQDs were obtained by varying the ablation time ranging from 1 min to 120 min. The resultant samples were then subjected to centrifugation for 3 hours and was later filtered using syringe filters (Millipore, 0.22μm pore size). The schematic diagram of preparation for GQDs from carboxyl-functional MWCNTs is shown on Fig. 1(a).
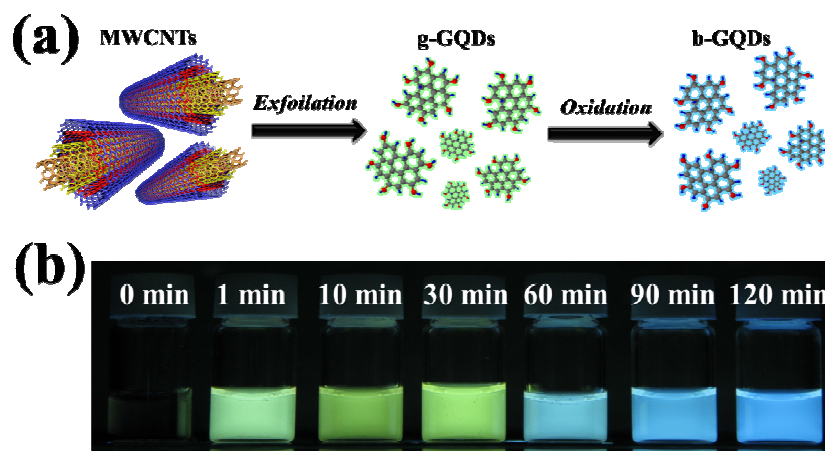
Fig. 1: (a) Schematic diagram of preparation of GQDs from carboxyl-functionalized MWCNTs and (b) images of the synthesized GQDs solutions under UV lamp at different PLA times.

For characterizing the structural properties of the as-synthesized GQDs, a high resolution transmission electron microscopy (HRTEM) (JEOL JEM-2100F) was used. X-ray photoelectron spectra (Thermo Scientific K-Alpha ESCA instrument) equipped with a monochromatized Al-Kα X-ray source at 1486.6 eV was used to determine the compositions of the GQDs. Ultraviolet-visible (UV-Vis) measurements were performed with the spectrophotometer (Varian Cary 50 UV) over a spectral range of 200-600 nm. A pulsed laser with a wavelength of 260 nm, duration of 250 fs, and repetition frequency of 20 MHz was used as the excitation source for studies of the steady-state and time-resolved PL. The collected PL was dispersed by a 0.75 m spectrometer and detected by the photomultiplier tube. Time-resolved PL techniques were carried out using time-correlated single-photon counting (TCSPC). The excitation-dependent PL spectra were analyzed using the spectrofluorometer (Horiba Jobin Yvon FluoroMax-4).

3. RESULTS AND DISCUSSION

After the PLA treatment of samples ranging from 1 to 120 min, each samples' color changes from pale purple to pale yellow under white light. The pale-yellow color of suspension was found to be similar to the GQDs prepared by other methods and may be

attributed to the disintegration of CNTs.[4,8,33] Fig. 1(b) shows photos of the suspension after different PLA time under UV light, displaying fluorescent light from green to blue color. The as-synthesized GQDs exhibit good water solubility, which is suggested to originate from the oxidation of the surface edges during laser ablation (will be shown later).

TEM was used to characterize and analyze the structures of the GQDs synthesized by PLA. Typical TEM images of samples under irradiation of laser for 10 and 120 min, referring as green and blue GQDs (gGQDs and bGQDs), are shown in Fig. 2(a) and Fig. 2(b), respectively. The size distributions of gGQDs and bGQDs are fitted by Gaussian curves and shown in Fig. 2c and Fig. 2d, respectively. Average diameters of 2.9±0.3 and 2.8±0.3 nm are respectively obtained for gGQDs and bGQDs by randomly counting more than 80 GQDs. HRTEM images (Fig. 2(e) and Fig. 2(f)) showed fine crystalline structures of the synthesized GQDs, displaying a clear lattice spacing of ~0.24 nm and ~0.23 nm for gGQDs and bGQDs, respectively. The GQDs size as well as their lattice spacing are in good agreement with those of TEM data synthesized from other methods.[6,14,26] In comparison to the existing synthesis method for GQDs, this synthesis method is one-step, green, fast, low cost, and environmental-friendly, and can be performed at room temperature in ambient atmosphere.
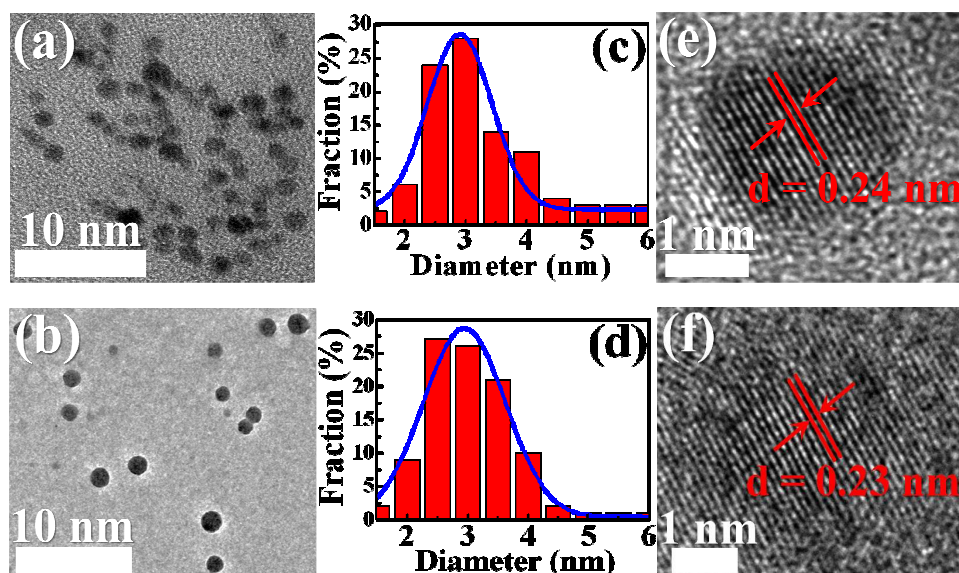

Fig. 2: TEM image, size distribution and HRTEM of (a, c, e) the GQDs synthesized by PLA for 10 min (gGQDs) and (b, d, f) the GQDs synthesized by PLA for 120 min (bGQDs), respectively.

It is well known that GQDs synthesized from the top-down method mostly exhibit green and/or blue luminescence.[10] Fig. 3(a) shows the PL spectra of the GQDs synthesized with different PLA time. The PL peak shifts toward the high-energy spectral region as the PLA time was increased. The gradual evolution of PL changes indicates that the tunable PL can be implemented by controlling the PLA time. Preparing GQDs with tunable PL is essential since variation of PL wavelength is desirable for many applications in optoelectronics. All the PL spectra in Fig. 3(a) can be deconvoluted into two Gaussian peaks, located at the wavelengths of 430 nm (blue emission) and 540 nm (green emission). For example, the PL from the GQDs synthesized by PLA for 10 min was deconvoluted as shown in Fig. 3(b). In Fig. 3(c), the intensity of green emission increases shortly with the PLA time from 0 to 10 min, then drastically decreases for further increase of PLA time. On the other hand, the intensity of blue emission increases monotonically as the PLA time increases. These observations indicate that the GQDs undergo a structural change during PLA.
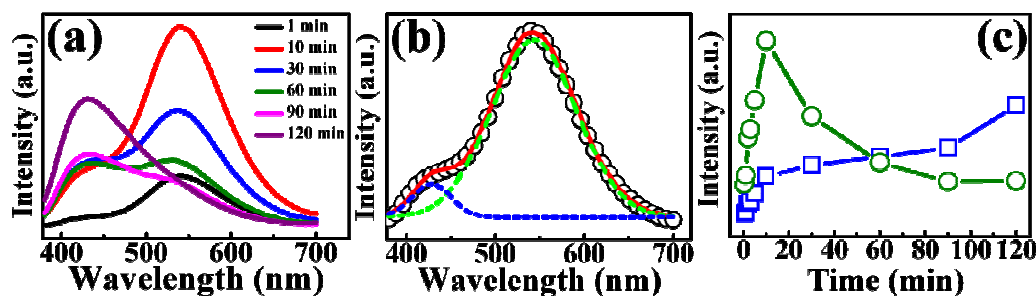

Fig. 3: (a) PL spectra of the GQDs generated by the different PLA time, (b) Deconvoluted Gaussian peaks from PL in GQDs synthesized by PLA for 10 min, and (c) evolution of the green and blue emission in GQDs generated by the different PLA time.

Fig. 4(a) shows the XPS survey of the GQDs synthesized at the PLA time of 10 min, indicating the GQDs consist of oxygen and carbon primarily. The C1s XPS spectra of GQDs synthesized with different PLA time are shown in Figs. 4(b)-4(g). The XPS spectra can be deconvoluted into three bands at the binding energies of 284.5, 286.2, and 288.4 eV, which corresponded to the sp^2 aromatic carbon (C=C), epoxy groups(C-O-C), and carboxyl groups

(C(O)-OH), respectively. A summary of percentage content of the GQDs extracted from Fig. 4(b) to Fig. 4(g) is shown in Fig. 4(h). It shows a decrease in the C=C structure and an increase of the epoxy as well of carboxyl contents as a function of the PLA time. This implies the oxygen containing functional groups on the surface of GQDs increase with respect to the increase of the PLA time. We therefore suggest that oxidation occurs during the PLA treatment, leading to an enhancement of oxygen containing functional groups such as epoxy and carboxyl groups. During the oxidation process, the graphitic structures could be cut into smaller pieces due to the epoxy chain-induced unzipping of carbon ring, which has been reported previously.[34] The oxidation due to PLA was further demonstrated using UV-Vis spectroscopy. As seen in Fig. 5, two distinct peaks appear in UV-Vis spectra with increasing PLA time, similar to those of GQDs synthesized using other methods.[8,18] The peak observed at ~220 nm was assigned to the π-π* transition of C=C bonds of aromatic sp^2 domains while the shoulder at ~330 nm was associated with GQDs.[4,8,18] The π-π* transition peak shifts toward the high-wavelength side significantly after the PLA treatment, evidencing the oxidation of the π-π* transition of aromatic sp^2 domains. Thus, the results from UV-Vis spectra also support the existence of oxidation after the PLA treatment.
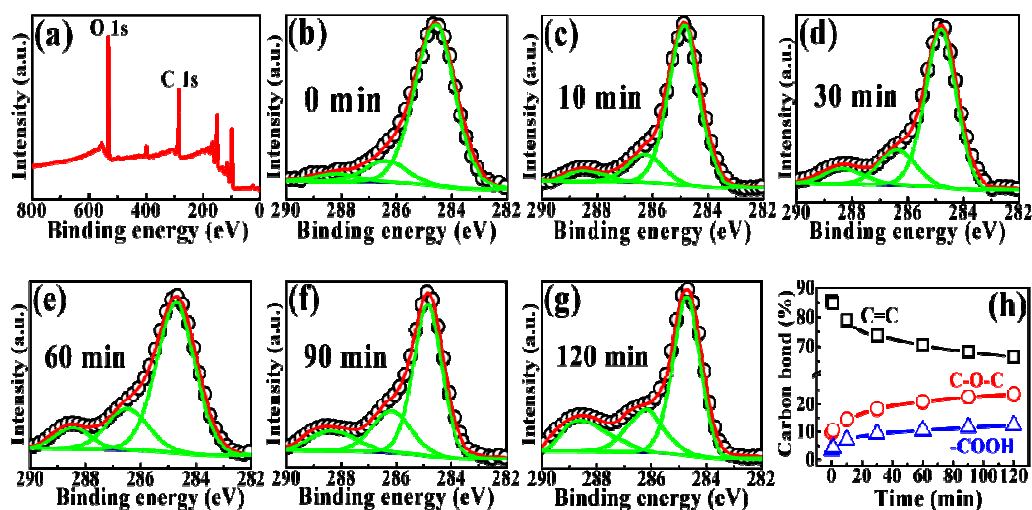

Fig. 4: (a) XPS survey of GQDs synthesized by PLA for 10 min, (b-g) C1s XPS spectra of GQDs generated by the different PLA time, and (h) carbon percentage content summary of the GQDs vs. the different PLA time.
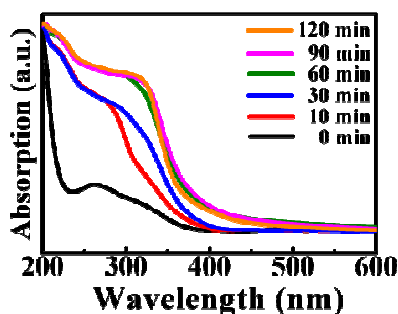
7

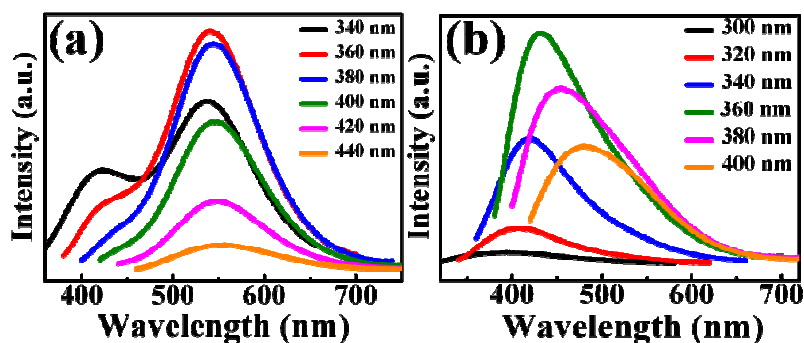Fig. 5: Absorption spectra of GQDs generated by the different PLA time.

Fig. 6: PL spectra of (a) gGQDs and (b) bGQDs with different excitation wavelengths.

The PL of GQDs and their luminescence mechanisms have been studied recently. The PL in GQDs has been associated with the free zigzag sites with carbene-like triplet states, π^*-π transitions of aromatic rings, edge states consisting of carbon atoms on the edge of carbon backbone, intrinsic transitions from sp^2 nanodomains, extrinsic transitions from the surface states, and interstate to band n-π induced transitions have been reported.[2,4,19,35] However, to date, the exact luminescence mechanism of GQDs is still an open question. This could be due to the complex PL origins of GQDs, which depends on their size, shape, edge type, surface configuration, solvent, and environment.[7,18] Fig. 6(a) shows the PL of gGQDs with respect to varying excitation wavelength, which displays an increased PL intensity for the excitation wavelength from 340 to 360 nm while a drastic decrease in PL intensity for the excitation wavelength over 380 nm. The peak energy of PL in gGQDs shows a negligible shift for a change of the excitation wavelength from 340 to 440 nm, exhibiting an excitation-independence PL characteristic. On the other hand, Fig. 6(b) shows the PL of bGQDs with

respect to a change of the excitation wavelength from 300 to 400 nm. A clear red-shift of the

PL peak with a varying intensity was observed for increasing the excitation wavelength. The

PL peak in bGQDs thus exhibits an excitation-dependence characteristic, different from that

in gGQDs. As previously reported, the excitation-dependent PL of the GQDs has been

attributed to the heterogeneity of its size, shape, defects, and composition of sp^2 domains as

well as the existence of interbands within the energy gap.[2,7] Here, the different excitation-

dependent behavior in Fig. 6a and Fig. 6b suggests that the PL in gGQDs and bGQDs have
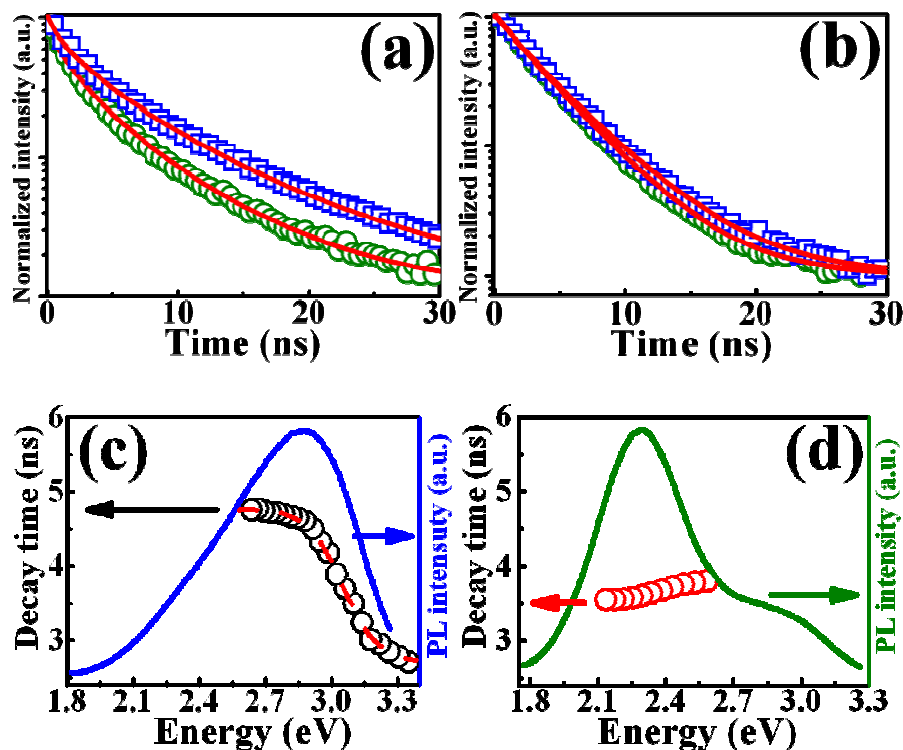
different origins.

Fig. 7: (a) Measured PL decay profiles of bGQDs with emission energy of 3.26 (open circles) and 2.76 eV

(open squares), respectively. (b) Measured PL decay profiles of gGQDs with emission energy of 2.17 (open

circles) and 2.52 eV (open squares), respectively. The solid lines in (a) and (b) are fits using Eq. (1). (c) and

(d) PL spectra (solid line) and emission energy dependence of PL decay times (open circles) obtained from

bGQDs and gGQDs, respectively. The dashed line in (c) is a fit to Eq. (3) from the carrier localization

model.

To investigate the luminescence mechanism, PL dynamics of gGQDs and bGQDs were studied. The open squares and circles in Fig. 7(a) and Fig. 7(b) display the PL decay profiles of the bGQDs and gGQDs, respectively. The PL decay curve is can be fitted by the stretched exponential function:

$$I(t) = I(0)e^{-(kt)^{\beta}} \quad , \quad (1)$$

where $I(0)$ is the initial PL intensity and k is the decay rate of PL intensity and β is a dispersive exponent. The fitted results are shown in the solid lines in Fig. 7a and Fig. 7b, in good agreement with experimental results. The average decay time of PL in the stretched exponential function is described by:

$$<\tau> = \frac{1}{k\beta}\Gamma(\frac{1}{\beta}) \quad , \quad (2)$$

where Γ is the Gamma function. The average decay time of PL in GQDs can thus be obtained from Eqs. (1) and (2). The open circles in Fig. 7(c) and Fig. 7(d) show the emission energy dependence of the average decay time of PL in bGQDs and gGQDs, respectively. It was found the average decay time of PL in bGQDs decreases with increasing emission energy, while that in gGQDs remains unchanged under different emission energies. The decrease of PL decay time with increasing emission energy is a characteristic of the carrier localization.[36] In the carrier localization mechanism, the carriers in the localized region can transfer from higher energy sites to lower energy sites before recombination. Hence, the decay rate of localized carriers is described as the radiative recombination rate plus the transfer rate to lower energy sites. On the basis of the carrier localization model, the PL decay time $\tau(E)$ as a function of emission energy can be expressed by:

$$\tau(E) = \frac{\tau_r}{1 + \exp[(E - E_{me})/E_0]} \quad , \quad (3)$$

where τ_r is the radiative lifetime, E_0 is the energy of the localization depth, and E_{me} is defined by an energy for which the decay time equals the transfer time. The emission dependence of PL decay time in bGQDs was fitted using Eq. (3) and plotted as the dashed red line in Fig.

10

7(c). A good fit to experimental data confirm that the blue PL in bGQDs is originated from recombination of the localized carriers. The emission energy dependence of the PL decay time gives an experimental evidence that the carrier localization effect are responsible for the blue PL in bGQDs. The localized states in the bGQDs may relate to the zigzag edges of GQDs since electrons in zigzag edges are exponentially localized near the Fermi level.[37] On the other hand, the PL decay time of gGQDs does not reveal a decrease with increasing emission energy, as shown in Fig. 7(d). This indicates the carrier localization effect is not evident for the green PL in gGQDs.
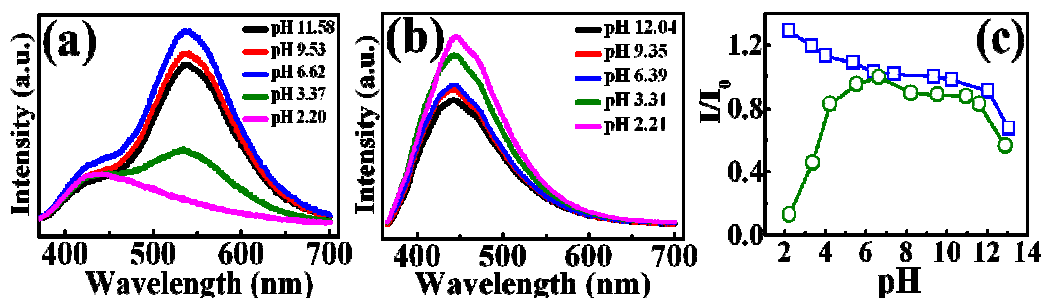

Fig. 8: (a) PL spectra of bGQDs with various pH values. (b) PL spectra of gGQDs with various pH values. (c) The integrated PL intensities of bGQDs and gGQDs as a function of pH values.

Fig. 8(a) and Fig. 8(b) display the PL spectra of bGQDs and gGQDs at different pH values, respectively. The intensity of the blue PL in bGQDs decreases as pH increased from 1.5 to 6.3 and from 10.5 to 13.0, while the PL intensity remains unchanged for pH 6.3-10.5. As for the green PL in the gGQDs, the emission intensity decreases with decreasing pH from 4.2 to 2.2 and with increasing pH from 11.4 to 13.0, and it remains constant for pH between 6.5 and 10.7. The PL intensities of bGQDs and gGQDs as a function of the pH value are shown in Fig. 8(c). In general, the change in the pH value of the solution ($[H^+]$ ion concentrations) can affect the oxygen containing functional group of GO or GQDs via protonation and deprotonation, leading to the inactivation and activation of the luminescence centers.[38-40] The increase of blue PL in the acidic conditions has been attributed to protonation of oxygen containing functional groups and passivation in the surface of GO, enhancing

11

symmetry of the π-π* state and reducing the nonradiative decay.[38] Another pH-dependence of

the blue PL in GO has been carried out and ascribed to the protonation from small numbers of

aromatic rings.[39] Thus, the blue PL in our bGQDs can be assigned to the intrinsic (core) state

associated with the sp^2 nanodomains. On the other hand, the green PL in GQDs has been

studied at different pH values, revealing a similar pH-dependent behavior to Fig. 8(b), i.e., a

decrease of PL in high and low pH value but a constant intensity in the pH values of 4-10.[40]

This trend has been ascribed to the protonation and deprotonation reactions of C=O functional

groups (carboxyl groups) at the edge of GQDs.[40] Therefore, we assign our green PL in

gGQDs to the extrinsic (edge) states embedded on the surface of GQDs. The above

assignments of the blue and green PL in GQDs can be further demonstrated by the following
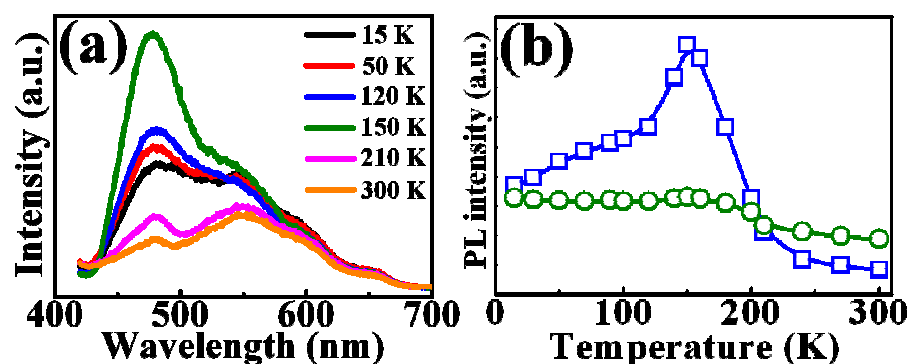
low-temperature PL studies.

Fig. 9: (a) PL spectra of solid-phase gGQDs at different temperatures. (b) Temperature dependence of PL intensities of bGQDs and gGQDs. The lines are guides for eyes.

The PL of the solid-phase gGQDs at low temperature was measured in the range from 15

to 300 K and shown in Fig. 9(a). All the PL spectra were deconvoluted into two Gaussian

peaks, including the blue and green emission. Fig. 9(b) displays a plot of the intensities of the

blue and green PL as a function of temperature. The temperature dependence of the blue PL

in GQDs is peculiar. The intensity of the blue PL increases as the temperature increases from

15 to 150 K, then it decreases sharply for temperatures higher than 150 K. We attribute the

temperature dependence of the blue PL from a recombination of self-trapped polaron excitons. Self-trapped polaron excitons with strong localization have been reported in molecular systerms such as fullerene C_{60} or light-harvesting complexes.[41-42] Upon excitation of photon with energy above the band gap (LUMO-HOMO gap), the photogenerated electrons and holes create a local lattice distortion and localize themselves into a state below the conduction band and above the valence band.[41] In raising temperatures (from 15 to 150 K), the transfer of excited electrons into of the localized polaron states increases due to an increase of thermal energy. This enhances a thermally activated radiative recombination in the localized polaron states and increases the intensity of the blue PL. At higher temperatures (over 150 K), the nonradiative recombination increases and the PL intensity decreases. Therefore, the blue PL in GQDs relates to the intrinsic (core) state which generates the local deformation in the lattice and produces a particular temperature effect in PL. The temperature dependence of the green PL exhibits a different behavior. The intensity of the green PL remains constant roughly from 15 to 150 K and decreases little after 150 K. The insensitive change of the green PL on temperatures suggests that the green PL originates from the extrinsic states or defect states.[43]

On the basis of the above investigations, a mechanism for the PL in GQDs is proposed. Upon photoexcitation, some of the photogenerated carriers in GQDs are produced and relax into the localized intrinsic states, originating from the sp^2 nanodomains. Subsequently, the carriers drop back to the ground state by radiative recombination processes and emit a blue PL in GQDs, as shown in Fig. 10 (left). On the other hand, the photogenerated carriers can be also captured by the extrinsic states embedded on the GQD surface, emitting the green PL (Fig. 10 (right)). As the MWCNTs treated with the PLA time from 1 to 10 min, the photo-induced oxidation produces localized sp^2 nanodomains and extrinsic edge states, generating the blue and green luminescence centers, respectively. When MWCNTs were treated with the PLA time from 10 to 120 min, the oxidation-induced cutting of the graphitic structure continues and the blue emission increases promptly. However, the oxidation process at this stage also produces lots of epoxy groups, which induce non-radiative recombination of

electron-hole pairs on the GQD surface.[38] Thus, the green PL of GQDs decreases as the PLA time more than 10 min. The excitation-dependent PL behavior in the blue PL of bGQDs can be also explained by the proposed model. Once the photogenerated carriers are captured in the localized states, the carriers can relax or be scattered into other localized states with lower energies. If the relaxation process keeps a finite lifetime, the carriers will recombine radiatively from higher localized states before they reach the lowest states. Thus, for those photogenerated carriers excited by the higher energy will relax to the lower localized states, then recombine and emit PL. This behavior produces a PL associated with the excitation energy (the excitation-dependent PL). On the other hand, the carriers in the delocalized states can only recombine at their sites since they have little chance to relax to other states, leading to an excitation-independence PL under excitation with different energies.
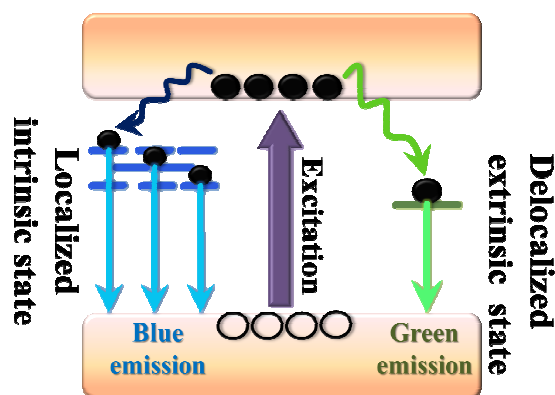

Fig. 10: Proposed PL mechanism of the GQDs synthesized with PLA

4. CONCLUSION

We have successfully demonstrated a top-down method of synthesizing GQDs from carboxyl-functionalized MWCNTs via PLA. The proposed method is one-step, low-cost, time-saving, and eco-friendly. The synthesized GQDs with an average size smaller than 3 nm were obtained by analysis of the TEM image. The physical and chemical properties of the as-synthesized GQDs were characterized by using TEM, XPS, UV-Vis, PL and time-resolved PL spectroscopy. The color of PL for the GQDs can be tunable from green to blue by varying

the PLA time. The PL of bGQDs shows the excitation-dependent characteristics upon photoexcitation with different wavelengths, attributing to the relaxation of the photogenerated carriers in the localized states. According to the investigations of pH- and temperature-dependent PL, the blue and green PL in GQDs have been attributed to the intrinsic (core) states related to the sp^2 nanodomains and the extrinsic (edge) states embedded on the GQD surface, respectively

Acknowledgments

References:

1. J. Peng, W. Gao, B. K. Gupta, Z. Liu, R. R. Aburto, L. Ge, L. Song, L. B. Alemany, X. Zhan, A. A. Marti, T. Hayashi, J. J. Zhu and P. M. Ajayan, *Nano Lett.*, 2012, **12**, 844-9.

2. G. S. Kumar, R. Roy, D. Sen, U. K. Ghorai, R. Thapa, N. Mazumder, S. Saha and K. K. Chattopadhyay, *Nanoscale*, 2014, **6**, 3384.

3. D. Pan, J. Zhang, Z. Li and M. Wu, *Adv. Mater.*, 2012, **22**, 734-738.

4. K. Habiba, V. I. Makarov, J. Avalos, M. J. F. Guinel, B. R. Weiner and G. Morell, *Carbon*, 2013, **07**, 084.

5. F. Liu, M. H. Jang, H. D. Ha, J. H. Kim, Y. H. Cho and T. S. Seo, *Adv. Mater.*, 2013, **25**, 3657-3662.

6. S. H. Jin, D. H. Kim, G. H. Jun, S. H. Hong and S. Jeon, *ACS Nano*, 2013, **7** (2), 1239-1245.

7. M. A. Sk, A. Ananthanarayanan, L. Huang, K. H. Lim and P. Chen, *J. Mater. Chem. C.*, 2014, **2**, 6954-6960.

8. L. Lin and S. Zhang, *Chem. Commun.*, 2012, **48**, 10177-10179.

9. S. Umrao, M. H. Jang, J. H. Oh, G. Kim, S. Sahoo, Y. H. Cho, A. Srivastva and I. K. Oh, *Carbon*, 2015, **81**, 514-524.

10. P. Yang, L. Zhou, S. Zhang, N. Wan, W. Pan and W. Shen, *J. Appl. Phys*, 2014, **116**, 244306.

11. B. P. Qi, H. Hu, L. Bao, Z. L. Zhang, B. Tang, Y Peng, B. S. Wang and D. W. Pang, *Nanoscale*, 2015, **7**, 5969.

12. W. Chen, F. Li, C. Wu and T. Huo, *Appl. Phys. Lett*., 2014, **104**, 063109.

13. L. Lin, M. Rong, F. Luo, D. Chen, Y. Wang and X. Chen, *J. Trac*, 20144, **54**, 83-102.

14. Y. Sun, S. Wang, C. Li, P. Luo, L. Tao, Y. Wei and G. Shi, *Phys. Chem. Chem. Phys*., 2013, **15**, 9907-9913.

15. Y. Dong, H. Pang, S. Ren, C. Chen, Y. Chi and T. Yu, *Carbon*, 2013, **64**, 245-251.

16. X. Zhu, X. Xiao, X, Zuo, Y. Liang and J. Nan, *Part. Part. Syst. Charact*., 2014, **31**, 801-809.

17. S. Wang, Z. G. Chen, I. Cole and Q. Li, *Carbon*, 2015, **82**, 304-313.

18. L. Li, G. Wu, G. Yang, J. Peng, J. Zhao and J. J. Zhu, *Nanoscale*, 2013, **5**, 4015.

19. L. Wang, S. J. Zhu, H. Y. Wang, S. N. Qu, Y. L. Zhang, J. H. Zhang, Q. D. Chen, H. L. Xu, W. Han, B. Yang and H. B. Sun, *ACS Nano*, 2014, **8**, 3, 2541-2547.

20. S. Zhu, J. Zhang, X. Liu, B. Li, X. Wang, S. Tang, Q. Meng, Y. Li, C. Shi, R. Hu and B. Yang, *RCS Adv*., 2012, **2**, 2717-2720.

21. Y. Dong, J. Shao, C. Chen, H. Li, R. Wang, Y. Chi, X. Lin and G. Chen, *Carbon*, 2012, **50**, 4738-4743.

22. X. T. Zheng, A. Ananthanarayanan, K Q. Luo and P Chen, *Small*, 2015, **11**, 14, 1620-1636.

23. J. Deng, Q. Lu, H. Li, Y. Zhang and S. Yao, *RSC Adv*., 2015, **5**, 29704-29707.

24. L. Wang, Y. Wang, T. Xu, H. Liao, C. Yao, Y. Liu, Z. Lin, Z. Chen, D. Pan, L. Sun and M. Wu, *Nature Commun*., 2014, **5**, 6357.

25. R. Ye, Z. Peng, A. Metzger, J. Lin, J. A. Mann, K. Huang, C. Xiang, X. Fan, E. L. G. Samuel, L. B. Alemany, A.A. Marti and J. M. Tour, *ACS Appl. Mater. Interfaces*, 2015, **7,** 7041-7048.

26. T. Fan, W. Zeng, W. Tang, C. Yuan, S. Tong, K. Cai, Y Liu, W. Huang, Y. Ming and A. J. Epstein, *Nano. Res. Lett*., 2015, **10**, 55.

27. M. Hassan, E. Haque, K. G. Reddy, A. I. Minett, J. Chen and V. G. Gomes, *Nanoscale*, 2014, **6**, 11988.

28. V. Amendola and M. Meneghetti, *Phys. Chem. Chem. Phys*., 2009, **11**, 3805-21.

29. L. Minati, S. Torrengo, D. Maniglio, C. Migliaresi and G Speranza, *Mater. Chem. Phys*., 2012, **08**, 071.

30. G. W. Wang, *Prog. Mater. Sci*., 2007, **52**, 648-698.

16

31. T. N. Lin, K. H. Chih, C. T. Yuan, J. L. Shen, C. A. J. Lin and W. R. Liu, *Nanoscale*, 2015, **7**, 708-2715.

32. R. Ye, C, Xiang, J. Lin, Z. Peng, K. Huang, Z. Yan, N. P. Cook, E. L. G. Samuel, C. C. Hwang, G. Ruan, G. Ceriotti, A. R. O. Raji, A. A. Martin and J. M. Tour, *Nature Commun.*, 2013, **4**, 2943-2948.

33. T. J. Simmons, J. Bult, D. P. Hashim, R. J. Linhardt and P. M. Ajayan, *ACS Nano*, 2009, **3**, 4, 865-870.

34. Z. Li, W. Zhang, Y. Luo, J. Yang and J. G. Hou, *J. Am. Chem. Soc.*, 2009, **131**, 6320-6321.

35. S. H. Song, M. H. Jang, J. Chung, S. H. Jin, B. H. Kim, S. H. Hur., S. Yoo. Y. H. Cho and S. Jeon, *Adv. Opt. Mater.*, 2014, **2**, 1016-1023.

36. T. Bartel, M. Dwaorzak, M. Strassburg, A. Hoffmann, A. Strittmatter and D. Bimberg, *Appl. Phys. Lett.*, 2004, **85**, 1946-1948.

37. I. Kleftogiannis, I. Amanatidis, and V. A. Gopar, *Phys. Rev. B*, 2013, **88**, 205414.

38. A. Gupta and S. K. Saha, *Nanoscale*, 2012, **4**, 6562-6567.

39. D. Kozawa, Y. Miyauchi, S. Mouri, and K. Matsuda, *J. phys. Chem. Lett.* 2013, **4**, 2035-2040.

40. L. Wang, S. Zhu, H. Wang, S. Qu, Y. Zhang, J. Zhang, Q. Chen, H. Xu, W. Han, B. Yang, and H. Sun, *ACS Nano*, 2014, **8,** 2541-2547.

41. M. Matus, H. Kuzmany, and E. Sohmen, *Phys. Rev. Lett.*, 1992, **68,** 2822-2825.

42. A. Freiberg, M. Rätsep, K. Timpmann, G. Trinkunas, and N. W. Woodbury, *J. Phys. Chem. B,* 2003, **107**, 11510-11519.

43. J. Fournier, P. Grua,1 J. Néauport, E. Fargin, V. Jubera, D. Talaga, A. Del Guerzo, G. Raffy, and S. Jouannigot, *Opt. Mater. Express,* 2013, **3**, 1-10.